Automatic identification of multiply diffracted waves and their ordered scattering paths

Katrin Löer,[a] Giovanni A. Meles, and Andrew Curtis
School of GeoSciences, The University of Edinburgh, Grant Institute, The King's Buildings, Edinburgh EH9 3FE, United Kingdom

(Received 30 August 2014; revised 5 January 2015; accepted 12 January 2015)

An automated algorithm uses recordings of acoustic energy across a spatially-distributed array to derive information about multiply scattered acoustic waves in heterogeneous media. The arrival time and scattering-order of each recorded diffracted acoustic wave, and the exact sequence of diffractors encountered by that wave, are estimated without requiring an explicit model of the medium through which the wave propagated. Individual diffractors are identified on the basis of their unique single-scattering relative travel-time curves (move-outs) across the array, and secondary (twice-scattered) waves are detected using semblance analysis along temporally offset primary move-outs. This information is sufficient to estimate travel times and scattering paths of all multiply diffracted waves of any order, and for these events to be identified in recorded data. The algorithm is applied to synthetic acoustic data sets from a variety of media, including different numbers of point-diffractors and a medium with strong heterogeneity and non-hyperbolic move-outs. © *2015 Acoustical Society of America*. [http://dx.doi.org/10.1121/1.4906839]

[RKS] Pages: 1834–1845

I. INTRODUCTION

The phenomenon of diffraction describes the interaction of propagating energy (e.g., acoustic and elastic waves, electromagnetic radiation, or moving particles) with sub-wavelength heterogeneities within the medium that are generally referred to as scatterers or diffractors (Born and Wolf, 1999). Diffractions play an important role in many fields of theoretical and applied acoustics, including medical imaging (Insana *et al.*, 1990; Tadayyon *et al.*, 2014), localization and destruction of kidney stones using medical ultrasound and lithotripsy (Fink *et al.*, 2003), ocean acoustics for the detection of marine organisms (Brekhovskikh and Lysanov, 2003; Foote, 2008), but also in other fields of physics including quantum mechanics (Friedrich, 2006), non-destructive testing (Prada *et al.*, 2002), remote sensing (Ferretti *et al.*, 2001), ground-penetrating radar (Papziner and Nick, 1998), near-surface geophysics (Harmankaya *et al.*, 2013; Kaslilar *et al.*, 2014), seismic exploration and monitoring (Landa *et al.*, 1987; Khaidukov *et al.*, 2004; Pacheco and Snieder, 2006; Halliday and Curtis, 2009; Halliday *et al.*, 2010; Jixiang *et al.*, 2014), and global seismology (Wu and Aki, 1988). In all such cases being able to predict or interpret diffracted energy is crucial.

Although in most applications the medium of interest contains multiple diffractors, it is often assumed that significant recorded wave energy has only scattered once, in order to simplify the wave theory considered. In that case, only energy that has interacted with a single diffractor is correctly taken into account. Apart from the fact that this assumption neglects many of the data which contain additional information about the medium, it may also lead to misinterpretation of the data and hence to incorrect conclusions. As examples in various fields of ongoing research show (Stanton, 1982; Gao *et al.*, 1983; Bordier *et al.*, 1991; De Rosny and Roux, 2001; Aubry and Derode, 2010), taking multiple scattering into account often leads to improved results. Some authors (Larose *et al.*, 2006; Aubry and Derode, 2010) also address the problem of separating singly from multiply scattered wavefields and analyzing the information content in different parts of the wavefield separately.

Recently, Meles and Curtis (2014a) presented a new method to identify multiply diffracted waves in acoustic data gathers. Moreover, it identifies all individual diffractors involved in the corresponding scattering path for each wave, and the sequential order in which they were encountered. It relies on *fingerprinting* individual diffractors in common-source gathers and common-receiver gathers (gathers are data subsets) by means of their unique move-out (travel time variation across arrays of receivers or sources, respectively). The method has a range of possible applications such as improved localization of diffractors or estimation of inter-scatterer medium properties, or discriminating physical from non-physical energy in wavefield interferometry (Meles and Curtis, 2014b); however, until now the method required substantial manual intervention. This is possible, though time-consuming, only in a medium of low complexity (with very few diffractors) and for data with very low noise levels.

We present an algorithm that *automatically* identifies primary and secondary waves (waves that have diffracted exactly once or twice, respectively), and *predicts* arrival times of higher-order multiply diffracted waves (those that have diffracted three times or more). The latter multiply-diffracted wave arrivals may then be identified in recorded data and associated with an exact scattering path, despite the method

[a]Author to whom correspondence should be addressed. Electronic mail: katrin.loer@ed.ac.uk

 0001-4966/2015/137(4)/1834/12/$30.00 © 2015 Acoustical Society of America

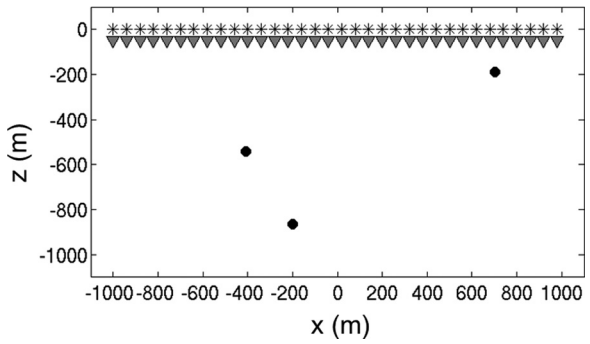

FIG. 1. Example geometry for a 3-diffractors model. Stars are sources, triangles are receivers, and black solid circles denote the locations of point diffractors. For clarity, only every third source and receiver is plotted. The velocity of the background medium is 1000 m/s.

requiring no explicit model of the medium or of the diffractor locations. In this paper we briefly revise the theoretical concept of the method of Meles and Curtis (2014a) and introduce the new automated algorithm that predicts the arrival times of multiply-scattered events in three steps: (1) Automatic estimation of primary travel-time curves (fingerprints) from common-source and common-receiver data gathers, (2) identification of secondaries on the mutual trace common to both gathers, and (3) prediction of travel times of all multiples up to any specified order by summing and subtracting primary and secondary travel times. We test the algorithm on a range of synthetic data sets involving different numbers of scatterers, varying noise-to-signal ratios, and non-hyperbolic move-outs. The results are compared to the true arrival times and scattering paths computed from the numerical models, and limitations of the method are addressed in Sec. V.

II. THEORY: FINGERPRINTING DIFFRACTORS

The fingerprint of an individual point diffractor corresponds to a unique travel-time curve across a common-receiver gather (CRG) or a common-source gather (CSG) (Meles and Curtis, 2014a). A CSG is the set of time series recorded at an array of receivers when the recorded energy has been generated by a single (common) source. Similarly, a CRG is the set of time series recorded between a single (common) receiver and an array of sources. Figure 1 shows the three-diffractors model that was used to generate an example of a synthetic CSG and a CRG [Fig. 2(a)] using an implementation of Foldy's method (Foldy, 1945; Galetti *et al.*, 2013). When both a source array and a receiver array are used, a *cube* of recorded data is generated defined by the sources along one axis, the receivers along another axis, and the recording time along the third axis [Fig. 2(b)]. Two crossing slices within this cube correspond to a CRG and a CSG, and have a mutual trace which is common to both gathers and is the record of the wavefield generated from the common source recorded at the common receiver [vertical bold line in Figs. 2(a) and 2(b)].

We refer to any distinctly observed arriving packet of energy as an *event*, and to the recorded time series at a single receiver as a *trace*. The travel time variations of a singly scattered wave (a primary) prescribe a so-called move-out along the traces of the CSG or CRG. The move-out gives the *relative* time of arrival of the diffracted wave as a function of receiver or source position, respectively, and is solely determined by the properties of the diffractor and the background medium, and the location of the diffractor with respect to the receiver array or the source array. Each diffractor can be related to a unique primary move-out, its so-called *fingerprint*. Meles and Curtis (2014a) show that this uniqueness also holds for inhomogeneous media, other than for pathological cases.

The number of distinct primary move-outs in the data (the CSG or CRG) corresponds to the number of diffractors in the illuminated part of the medium. Further, multiple occurrences of the same move-out arriving at different times

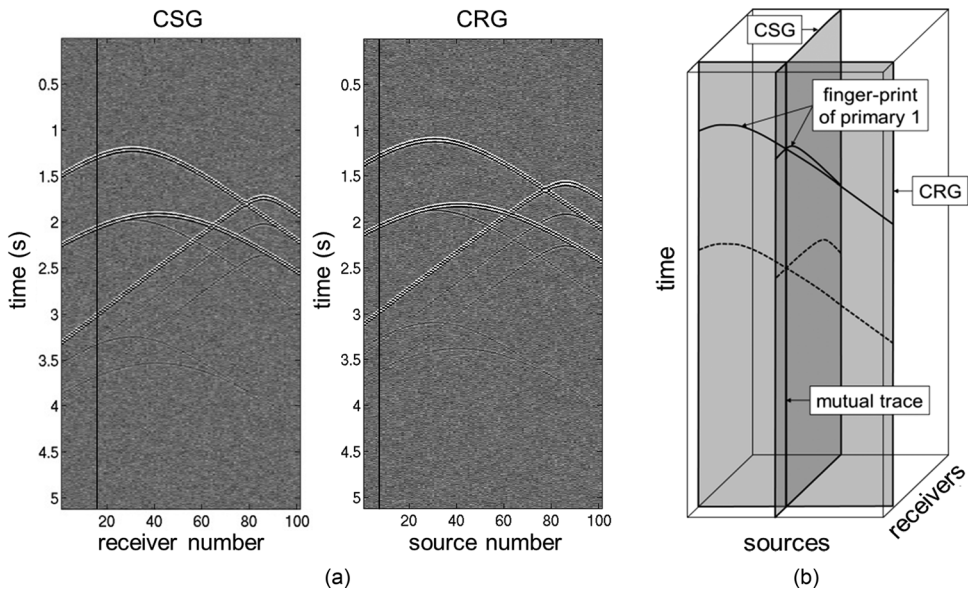

FIG. 2. (a) Synthetic CSG (left) and CRG (right) obtained using the 3-diffractors model shown in Fig. 1 with the common source located at [−880 m, 0 m] and the common receiver located at [−680 m, −50 m], respectively. The noise-to-signal ratio is 0.5, where a ratio of 1 means that the root-mean square noise is equal to the typical amplitude of a secondary (a twice-scattered wave). (b) The data-cube showing a CSG and a CRG as two orthogonal (schematic) sections. The vertical bold line in both panels of (a) marks the mutual trace that is common to both of the gathers, and this is denoted also in the schematic gathers in (b).

indicate multiply scattered events. In a CSG, multiply scattered waves can be classified by the *last* diffractor they have visited: The move-out curve of any multiply scattered wave with last diffractor L is equal to that of the primary of L, with an additional constant travel-time shift that accounts for the longer ray path before visiting diffractor L [Fig. 3(a)]. Hence, all events with the same last diffractor have the same move-outs in a CSG. In a CRG, all events can be classified similarly according to the *first* diffractor along the scattering path [Fig. 3(b)]. Combining the information from both gathers on any chosen mutual trace (that is common to both gathers) we can identify the first and last diffractor along the scattering path for any event observed on the trace: Thus, every event observed on any chosen trace can be associated with a move-out pair, namely the fingerprints of the first and last diffractor. This is important because primaries and secondaries can all be identified uniquely as the first events on the recorded trace associated with a particular move-out pair: For primaries both move-outs match the fingerprints of the same (single) diffractor, while for secondaries the source and receiver move-outs match the fingerprints of different first and last diffractors.

Meles and Curtis (2014a) show that one can then choose an arbitrary event on any trace and analyze the sequential order of diffractors involved in its scattering path. The last diffractor L in the scattering path is classified according to its move-out as shown above. The penultimate diffractor, $L-1$, is identified by using a particular combination of cross-correlation and convolution of primaries and secondaries (or by a combination of additions and subtractions of their travel times). By induction, the diffractors $L-2$, $L-3$, and so on are identified similarly until the full scattering path of any chosen event is recovered.

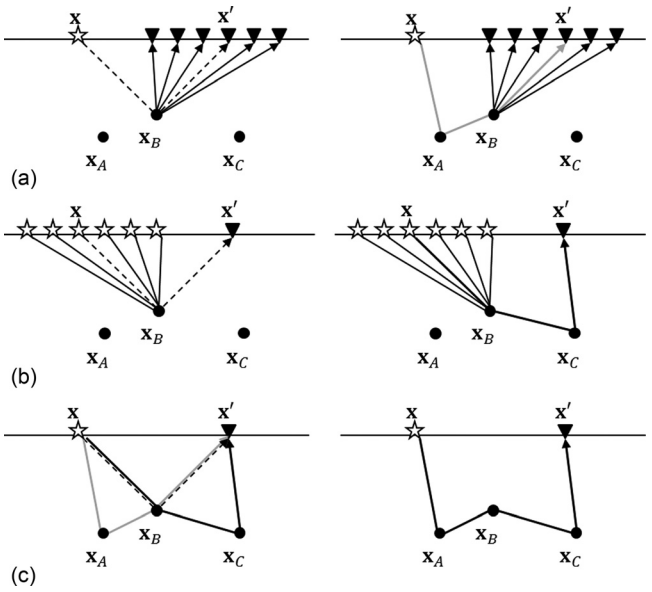

FIG. 3. Schematic construction of multiply diffracted events from primaries and secondaries. Symbol key as in Fig. 1. (a) CSG: Ray paths of the primary scattered at $\mathbf{x}_B$ and of the secondary with first diffractor $\mathbf{x}_A$ and last diffractor $\mathbf{x}_B$. Note that the receiver-side move-outs are the same. (b) CRG: Ray paths of the primary scattered at $\mathbf{x}_B$ and of the secondary with first diffractor $\mathbf{x}_B$ and last diffractor $\mathbf{x}_C$. Note that the source-side move-outs are the same. (c) Events on the mutual trace that are used to estimate the travel time of a tertiary scattered event: Two secondaries (gray and bold) are convolved and the result is cross-correlated with a primary (dashed). Travel times along dashed and solid ray path components that follow the same paths cancel each other as a result of cross-correlation. This operation gives the travel time of the tertiary event scattered sequentially at diffractors $\mathbf{x}_A$, $\mathbf{x}_B$, and $\mathbf{x}_C$.

The method requires that the move-out of the event can be classified uniquely on both the CSG and the CRG. This can be difficult especially for late arriving waves that undergo higher-order scattering, have low amplitudes, and are embedded in a complex wavefield where individual move-outs may not be distinguishable. Nevertheless, the method has been demonstrated successfully for scattering events up to fourth order in a noise-free synthetic acoustic data set; that is, the scattering path of any observed event could be interpreted provided the energy in that event had not scattered more than four times.

In this work we implement, automate, and demonstrate the reverse process to that of Meles and Curtis (2014a): Rather than analyzing scattering paths of events observed on the recorded trace, our method *predicts* travel times of all multiply diffracted waves [Fig. 3(c)], which can then be identified in recorded data. In fact, this method was proposed schematically by Meles and Curtis (2014a), but was neither implemented nor tested.

III. THE AUTOMATED SCHEME

Automation of the new algorithm requires a method to detect move-outs of different diffractors, and repetitions of the same move-out across each gather. It should be applicable to either simple or complex wavefields where the human eye may not be able to recognize individual move-outs. We now describe three stages in an algorithm that achieves this.

A. Isolating primary move-outs using cross-correlation of gathers

We first isolate and identify the primary move-outs, which provide the basis for all further analyses. To do so, we exploit the fact that the shape of a primary diffracted move-out in a CSG is invariant with respect to the source position apart from a constant shift in time. That is, if we compare a CSG to a second such gather with a different source position, we will find the same primary move-out curves in the second gather, but each curve will be shifted by a different amount along the time axis [Figs. 4(a) and 4(b)]. This assumption applies equally to CRGs with respect to location of the receiver.

The invariance of diffraction move-outs across multiple CSGs allows us to isolate them from the rest of the data and estimate their arrival-time curves using cross-correlation. Standard cross-correlation allows one to estimate the time shift between two traces under which they are most alike with respect to a squared norm. We wish to find similarities between two gathers (A and B_1, say) rather than two individual traces, so we first perform cross-correlation between each pair of traces at each receiver in the two gathers, then sum the results over receivers. This can be written in the time domain for discrete time samples i as

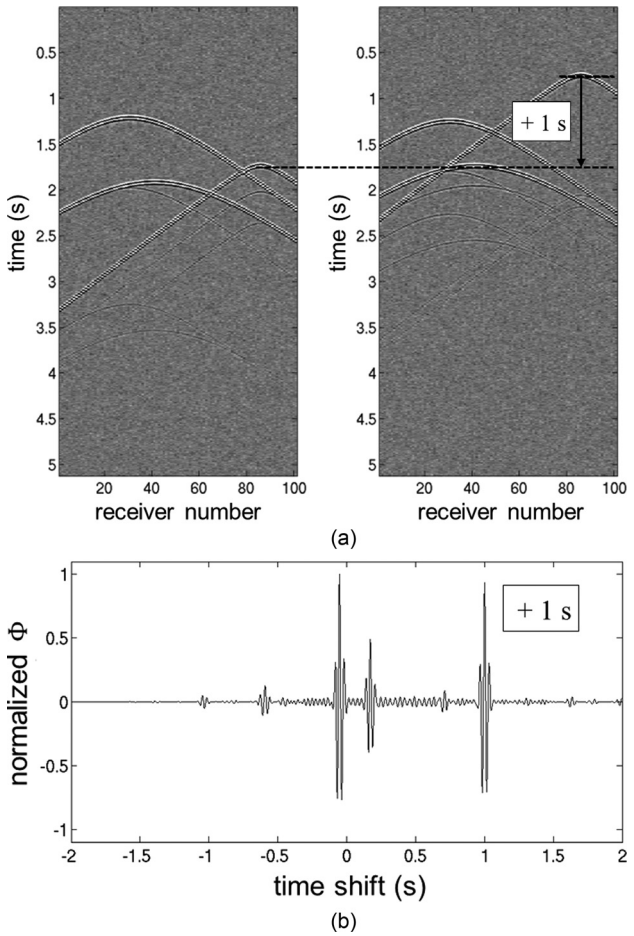

FIG. 4. (a) Two CSGs with sources located at [−880 m, 0 m] and [−380 m, 0 m] in Fig. 1, respectively, and a noise-to-signal ratio of 0.5. Both gathers contain the same three primary move-outs (fingerprints of each of the three diffractors in Fig. 1), but shifted in time (i.e., vertically up or down the gather) due to the change in source position. As an example the dashed lines indicate the shift by 1 s of the rightmost move-out. (b) Result of cross-correlation [Φ_1 in Eq. (1)] between the two gathers shown in (a). Time lag i in Eq. (1) has been converted to seconds. The peaks indicate the three time shifts under which both gathers are most alike with the peak at 1 s corresponding to the shift of the rightmost move-out in both gathers. These time shifts are used to isolate the individual move-outs from the left gather in (a).

$$\Phi_1(i) = \sum_{m=1}^{\min(M_A,M_B)} \sum_{n=1}^{N} A(m,n)B_1(m+i,n), \tag{1}$$

where $\Phi_1(i)$ denotes the correlation coefficient at time shift i, M_A and M_B are the record lengths in gathers A and B_1, respectively, and N is the number of traces in each gather. In gather $A(m,n)$, for example, m is the time index and n is the receiver index.

Φ_1 has its maximum recorded amplitude at time shift $i = i_1$, say, for which A and B_1 are most alike. i_1 is usually the time by which one of the recorded primary move-outs (typically the one with the largest amplitude) is shifted between gathers A and B_1 due to the relative shift in source position [Fig. 4(b)]. To identify this particular move-out, gather B_1 is shifted in time by i_1 and multiplied element-wise with gather A according to

$$C_1(m,n|i=i_1) = A(m,n)|B_1(m+i_1,n)|. \tag{2}$$

Ideally, the resulting cross-gather C_1 has maximum values along the primary move-out associated with time shift i_1: All other elements should have close to zero amplitudes [Fig. 5(a)]. However, when the data are noisy or contain many intersecting move-outs, residual energy that is not related to that move-out remains in the cross-gather and affects the accuracy of the estimated move-out. To attenuate this energy, the cross-gather is correlated with a new CSG, B_2, say. The maximum amplitude of that correlation function indicates the time-shift between the move-out in the cross-gather and the equivalent primary move-out in gather B_2, and therefore allows one to compute an updated cross-gather according to Eq. (4) below. This process is repeated iteratively, each iteration consisting of three steps initiated by setting $C_0 = A$ and $j = 1$:

(1) Cross-correlate two gathers (one of which is the previously determined cross-gather C_j) according to

$$\Phi_{j+1}(i) = \sum_{m=1}^{\min(M_A,M_B)} \sum_{n=1}^{N} C_j(m,n|i=i_j)B_{j+1}(m+i,n), \tag{3}$$

and identify the time shift i_{j+1} with the largest correlation coefficient.

(2) Multiply the two gathers element-wise—one of them shifted by the time shift i_{j+1} determined in (1)—to produce a new cross-gather according to

$$C_{j+1}(m,n|i=i_{j+1}) = C_j(m,n|i=i_j)|B_{j+1}(m+i_{j+1},n)|. \tag{4}$$

The cross-gather should have maximum values along the primary move-out associated with time shift i_{j+1}; all other elements should have close to zero amplitudes.

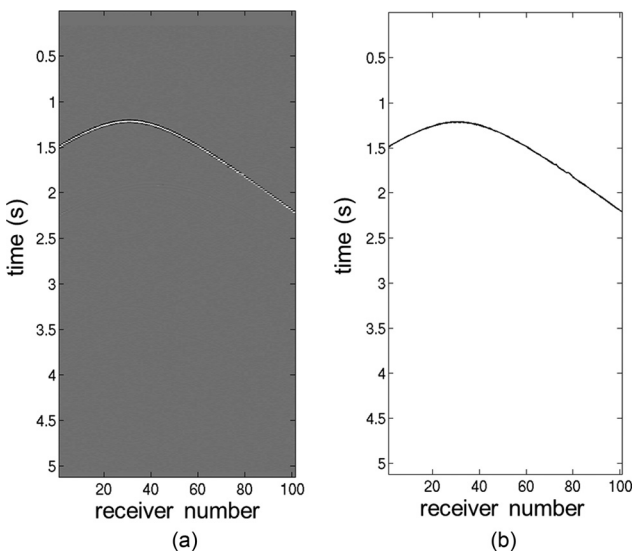

FIG. 5. (a) Cross-gather C for an initial time lag of −0.05 s [Eq. (2)] showing a single move-out isolated from the CSG in Fig. 4(a). (b) The identified travel-time curve as a function of receiver position estimated from (a) using Eq. (5).

(3) Estimate the corresponding travel-time curve as a function of receiver position by picking the maximum amplitude arrival on each trace of the cross-gather [Fig. 5(b)]

$$t_j(n|i=i_j) = \arg\max_m(|C_j(m,n,|i=i_j)|). \quad (5)$$

The energy along the primary move-out in the cross-gather in step (2) should be amplified in each iteration, producing a successively better estimate of the primary travel-time curve. Iterations cease when the estimated travel-time curve does not exhibit significant changes compared to that in the previous iteration.

So far the algorithm identifies one move-out, namely that which exhibits the largest correlation coefficient Φ_1. To find other diffraction move-outs we use an additional macro-iterative loop: At the beginning of each macro-iteration, recorded energy with previously detected move-outs is removed from the original CSG (gather A) by muting all traces around the identified arrival-time curves. The muted gather is then used in the initial correlation step [Eq. (1)]. However, when computing the first cross-gather using Eq. (2), the original (unmuted) CSG is used in order to avoid gaps in the move-out energy due to muting, which would result in discontinuous arrival-time estimates. Thus we iteratively find successive move-out curves.

The search for additional move-outs ceases when the maximum of Φ_1 falls below a certain threshold, here defined as $\Phi_1(i_1) * 0.1 * 0.9^l$, where $\Phi_1(i_1)$ is the maximum of the first correlation coefficient and l is the number of move-outs already detected and removed from the gather. This dynamic threshold accounts for the fact that in each iteration the total amount of energy in the gather is reduced by muting. The two variable parameters (0.1 and 0.9) are chosen empirically and depend on the relative locations and scattering amplitudes of the diffractors, as well as on the noise level. The influence of this threshold on the results is explained in more detail in Sec. V.

Note that the initial gather A can be chosen arbitrarily, although certain source locations may provide a better illumination angle (resulting in fewer intersections or larger amplitudes of diffracted energy) depending on the distribution of diffractors in the medium with respect to the source and the receiver array. Nevertheless the identified move-outs should be identical and the estimated arrival-time curves only vary in absolute travel times, so that a comparison of the move-outs obtained from different initial gathers could be used to check the accuracy of results.

The method is, in principle, able to estimate travel-time curves of arbitrary complexity. Below we will show synthetic data examples containing non-hyperbolic move-outs obtained from a numerical model with a highly heterogeneous background velocity distribution. Note that the background medium has to be sufficiently smooth in order not to generate diffracted or reflected energy, i.e., velocity or density variations should occur over length scales significantly larger than the typical wave length.

The identification of primaries is carried out on both the CSG and the CRG. We then check if any two (or more) primaries arrive close to simultaneously on the mutual trace that is common to both gathers. If this is the case, a new trace is picked and the process is repeated until a suitable trace is found for which all primary arrivals are separated by at least the length of a wavelet. This reduces ambiguity about which common-receiver and common-source move-outs correspond to the same event. The mutual trace is chosen quasi randomly from different sub-sets ("bins") of the data cube, each containing 25 sources and 25 receivers in the examples herein. By testing traces from different bins we make sure that a variety of illumination angles are considered, which accelerates the search for a suitable mutual trace.

B. Detecting multiples using semblance analysis

The travel-time curves estimated from the cross-gathers are used to detect multiples with the same fingerprint, hence the same last (first) diffractor, arriving at later times in the CSG (CRG). This is achieved using semblance analysis, a technique commonly used in seismic velocity analysis (Thorson and Claerbout, 1985; Sheriff and Geldart, 1995). The semblance denotes the ratio of the total energy of the stack (sum) of energy in traces around a travel-time curve to the sum of the energy of the individual traces (Sheriff and Geldart, 1995). In our case the shape of the travel-time curve is already known and the only unknown parameter is a constant time shift t_{shift} between a primary and a multiple. The primary travel time curve $t(x)$ is shifted across the gather by t_{shift}, and the semblance S along the curve $t(x) + t_{\text{shift}}$ is computed according to

$$S(t_{\text{shift}}) = \frac{1}{N} \frac{\sum_{t_w=-(m/2)\Delta}^{(m/2)\Delta} \left[\sum_{x=1}^{N} g(t(x)+t_{\text{shift}}+t_w;x)\right]^2}{\sum_{t_w=-(m/2)\Delta}^{(m/2)\Delta} \sum_{x=1}^{N} [g(t(x)+t_{\text{shift}}+t_w;x)]^2}, \quad (6)$$

where N is the number of traces, and $g(t(x) + t_{\text{shift}} + t_w; x)$ is the value of trace x at time $t(x) + t_{\text{shift}} + t_w$, where t_w runs over the temporal length of the semblance window according to the outer summation in Eq. (6). Stacking over a time window of width $m\Delta$, where m is a positive scalar and Δ is the inverse of the temporal sampling rate, accounts for the fact that a coherent arrival on each trace extends over a finite time interval, namely roughly the length of the source wavelet. Due to the normalization factor $1/N$ values for S range between 0 and 1. When S is close to 1, all amplitudes sum coherently and the proposed travel-time curve $t(x) + t_{\text{shift}}$ fits a move-out that exists in the gather. The time shifts t_{shift} for which S is large thus provide the arrival times of multiples with the same last (or first) scatterer as the primary described by the travel time curve $t(x)$ (i.e., all arrival times are relative to the corresponding primary arrival). An example is shown in Fig. 6.

In order to increase the amplitudes of weak arrivals (especially secondaries) and equalize amplitudes across the whole move-out, a temporally adaptive gain was applied to the data before performing semblance analysis. This maintains the relative amplitudes of all arrivals in a specified time window (gain window) but normalizes the maxima of all

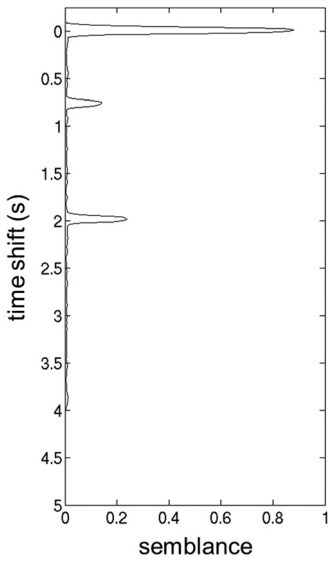

FIG. 6. Result of semblance analysis [$S(t_{\text{shift}})$ in Eq. (6)] for a CSG [Fig. 4(a)] using the travel-time curve shown in Fig. 5(b) at different time shifts. Time shifts are relative to the arrival time of the primary, represented by the peak at 0 s. The two later peaks indicate arrivals of multiples with the same move-out and hence the same last scatterer.

time windows. If the gain window is sufficiently small, this process sets all arrivals on a trace to the same amplitude including primaries and multiples, but also acts similarly on noise. For the semblance analysis, however, the amplitude of the noise is not important, assuming that it is incoherent in phase and therefore should not sum constructively. In our examples a gain window equivalent to the length of the wavelet provided the best results for noisy data.

Having identified the first diffractor of each event on the CRG, and the last diffractor of each event on the CSG, we combine these pieces of information on the mutual trace, which allows us to identify all secondary events: These are the first arriving events associated with each pair of different common-source and common-receiver move-outs (see Sec. II).

C. Predicting travel times of higher-order multiples

Once all primary and secondary events have been identified they can be used to construct any tertiary multiply scattered arrival by combining three events:

(1) Any primary,
(2) a secondary associated with the same *last* diffractor as the primary [Fig. 3(a)],
(3) a secondary associated with the same *first* diffractor as the primary [Fig. 3(b)].

The travel times of the two secondaries are added, and the travel time of the primary is subtracted, which yields the travel time of a tertiary arrival that should be able to be observed on the trace. The events that were used in the construction process also define the scattering path of the tertiary arrival: This is the concatenation of the scattering paths of the two secondaries (minus one instance of the common scatterer). We can go through this example using the vector scattering paths of three events traveling between a source at $\mathbf{x}$ and a receiver at $\mathbf{x}'$ as shown in Fig. 3(c):

(1) A primary scattered at diffractor $\mathbf{x}_B$ [scattering path $\overline{\mathbf{x}\mathbf{x}_B} + \overline{\mathbf{x}_B\mathbf{x}'}$],
(2) a secondary scattered at diffractors $\mathbf{x}_A$ and $\mathbf{x}_B$ [scattering path $\overline{\mathbf{x}\mathbf{x}_A} + \overline{\mathbf{x}_A\mathbf{x}_B} + \overline{\mathbf{x}_B\mathbf{x}'}$],
(3) and a secondary scattered at diffractors $\mathbf{x}_B$ and $\mathbf{x}_C$ [scattering path $\overline{\mathbf{x}\mathbf{x}_B} + \overline{\mathbf{x}_B\mathbf{x}_C} + \overline{\mathbf{x}_C\mathbf{x}'}$].

Adding and subtracting the travel times as described informally above then corresponds to finding the travel time after adding and subtracting vector scattering path components

$$(\overline{\mathbf{x}\mathbf{x}_A} + \overline{\mathbf{x}_A\mathbf{x}_B} + \overline{\mathbf{x}_B\mathbf{x}'}) + (\overline{\mathbf{x}\mathbf{x}_B} + \overline{\mathbf{x}_B\mathbf{x}_C} + \overline{\mathbf{x}_C\mathbf{x}'}) - (\overline{\mathbf{x}\mathbf{x}_B} + \overline{\mathbf{x}_B\mathbf{x}'}) = \overline{\mathbf{x}\mathbf{x}_A} + \overline{\mathbf{x}_A\mathbf{x}_B} + \overline{\mathbf{x}_B\mathbf{x}_C} + \overline{\mathbf{x}_C\mathbf{x}'}. \quad (7)$$

Hence, the tertiary with the predicted travel time is the one that has encountered the three diffractors in the sequential order $\mathbf{x}_A$, $\mathbf{x}_B$, and $\mathbf{x}_C$ as shown on the right of Fig. 3(c).

Subsequently, the travel times of higher-order multiples can be computed by replacing one of the secondaries with a tertiary in the above construction process. This process allows the travel times of multiply scattered waves of any order to be predicted, and each can be verified by direct observation of that multiple's move-out in the data. We will show that the time of arrivals can be predicted correctly even if the arrivals themselves are buried in a complex noise field.

Figure 7 displays the mutual trace of the 3-diffractors example obtained from the model in Fig. 1 with white noise added with a noise-to-signal ratio of 0.5 (where a ratio of 1 means the root-mean square noise is equivalent to the typical amplitude of a secondary arrival): here, all primary and secondary arrivals have been identified correctly by the algorithm (see Tables I and II) and the resulting prediction for third and fourth order multiples are also marked in the figure. The computing time required to analyze one such trace in this example is on the order of 1 min on a standard desktop computer, though finding a suitable mutual trace in the data cube requires additional time (up to 1 min for each trace that is tested). For increasing numbers of primary move-outs (i.e., numbers of diffractors in the model) the computing time also increases.

IV. NUMERICAL EXAMPLES

We test the automated algorithm on a range of synthetic data sets obtained from different two-dimensional (2D) acoustic models containing multiple isotropic point scatterers embedded in a homogeneous background medium (density $\rho = 1000\,\text{kg/m}^3$, velocity $v = 1000\,\text{m/s}$). A variety of Foldy's method embodied within a freely available wavefield modeling code (Foldy, 1945; Galetti *et al.*, 2013) is used to compute the diffracted wavefields including all orders of multiple scattering. Direct wave arrivals are not modeled since they have no interactions with the diffractors. In our example, source and receiver arrays consist of 101 sources and 101 receivers, respectively, and have the same lateral extension and the same horizontal spacing of 20 m (however, this is not a requirement of the method).

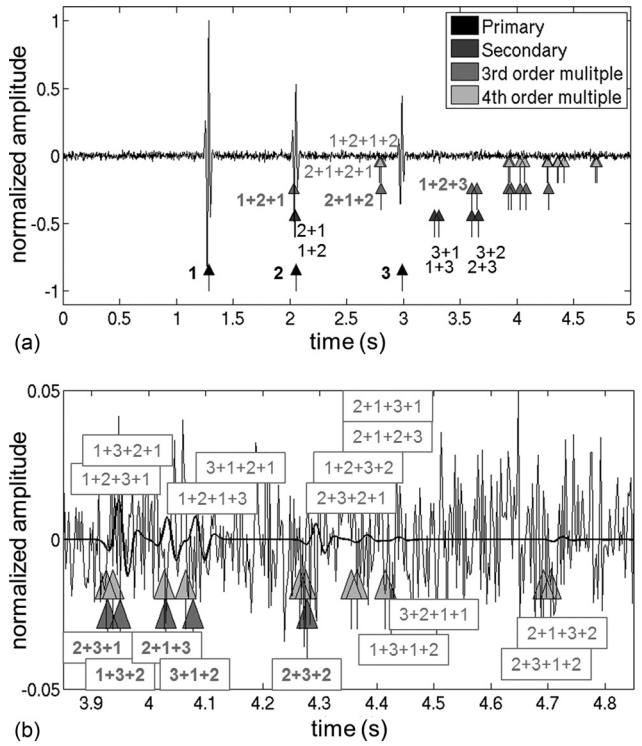

FIG. 7. (a) Mutual trace of the CSG and CRG shown in Fig. 2. The maximum amplitude has been normalized to one. Arrows mark the arrivals of estimated primary, secondary, third order, and fourth order events. In this example the algorithm detected all primaries and secondaries correctly (Tables I and II), i.e., the deviation from the true arrival time was below half the length of a wavelet (0.05 s); hence, all higher-order events are estimated within permitted accuracy. Numbers indicate the scattering path of individual events (up to 3.6 s), e.g., $3+1$ means a secondary scattered first at diffractor 3 and then diffractor 1. (b) Zoom on the trace in (a) between 3.85 and 4.85 s superimposed by the noise-free trace (bold) amplified by a gain of 4 to highlight small amplitude third and fourth order scattered arrivals embedded in the noise but predicted correctly by the algorithm.

Our aim is to demonstrate the performance of the algorithm in detecting primary and secondary arrivals correctly for (1) models containing varying numbers of diffractors, and (2) different noise-to-signal ratios. In our algorithm the prediction of higher-order multiples depends solely on the correct identification of primaries and secondaries. The number of diffractors in the model (between two and five) is predefined in each example; the locations of the diffractors are chosen randomly within a box of 2000 m $\times$ 1000 m beneath the source array and the receiver array (roughly the area shown in Fig. 1), such that the apexes of all move-outs are well-defined by the recorded data. The only other constraint is that the distance between any two diffractors is larger than twice the typical wavelength $\lambda \approx 33$ m so that each produces identifiable scattered wave energy.

TABLE I. Comparison of estimated (t_{est}) and true travel times (t_{true}) of primary arrivals on the mutual trace in the 3-diffractors example (Fig. 7). All estimated travel times lie within the permitted deviation of half the length of a wavelet (0.05 s).

Primary	t_{est}	t_{true}	$\lvert t_{est} - t_{true}\rvert$
1	1.29 s	1.28 s	0.01 s
2	2.05 s	2.05 s	0.01 s
3	2.99 s	2.98 s	0.01 s

TABLE II. Comparison of estimated (t_{est}) and true travel times (t_{true}) of secondary arrivals on the mutual trace in the 3-diffracors example (Fig. 7). All estimated travel times lie within the permitted deviation of half the length of a wavelet (0.05 s).

Secondary	t_{est}	t_{true}	$\lvert t_{est} - t_{true}\rvert$
$2+1$	2.04 s	2.05 s	0.01 s
$1+2$	2.05 s	2.05 s	0.00 s
$1+3$	3.28 s	3.27 s	0.00 s
$3+1$	3.31 s	3.32 s	0.01 s
$2+3$	3.60 s	3.61 s	0.01 s
$3+2$	3.66 s	3.66 s	0.00 s

For each set number of diffractors we test the algorithm on 15 different models, all containing the same number of diffractors but in different random locations. For each model we count the number of secondaries detected by the algorithm, and determine how many of them are predicted correctly (at the correct travel time on the mutual trace) and how many are incorrect. For comparison we use the true travel times of primary and secondary waves computed directly from the model. An event is classified as incorrect if the estimated travel time deviates by more than half the length of a wavelet from the true travel time. To test the influence of the choice of the mutual trace, we examine three different such traces for each model.

Next, we contaminate each data set with increasing noise-to-signal ratios (between 0.1 and 5, where a ratio of 1 means that the root-mean square noise is equal to the typical amplitude of a secondary), and for each we again count the number of primaries and secondaries detected correctly and those detected incorrectly. This process is repeated for different numbers of diffractors and the results are tabulated. A summary for primary and secondary events is given in Fig. 8, since travel times of all subsequent multiples depend only on these results as shown above and in Meles and Curtis (2014a).

To demonstrate that neither the isolation of primaries nor the detection of secondaries is restricted to media with homogeneous background velocities and hence data with hyperbolic move-outs, we include an illustrative example for data that exhibit clearly non-hyperbolic move-outs. This was created using a finite-difference modeling code with absorbing boundaries and a Ricker wavelet with central frequency of 30 Hz. Three randomly placed diffractors are represented as locations of high density contrast (3000 kg/m^3 and 1000 kg/m^3 in the background) and the velocity varies according to a smooth checkerboard pattern between 1500 and 2000 m/s (Fig. 9). The acquisition geometry is identical to that in previous examples and no noise is added to the data. Figure 10 shows a typical CSG from this experiment and the identified primary move-outs. Primary and secondary travel times as determined by our algorithm are compared to the true travel times calculated from the finite-difference model in Fig. 11 and Tables III and IV.

V. DISCUSSION

The identification of primaries by cross-correlation of two gathers is successfully carried out in over 90% of the cases even for several diffractors and relatively high noise-

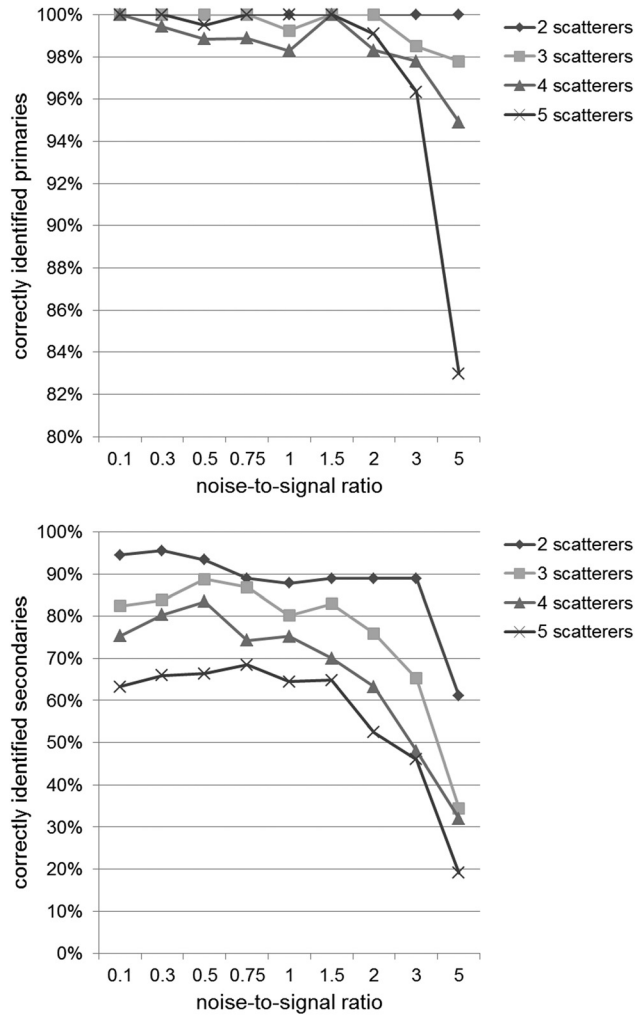

FIG. 8. Percentage of primaries (top) and secondaries (bottom) identified correctly (i.e., with the correct travel time, to within an accuracy limit of half of the source wavelet length) for different numbers of diffractors in the model and different noise-to-signal ratios.

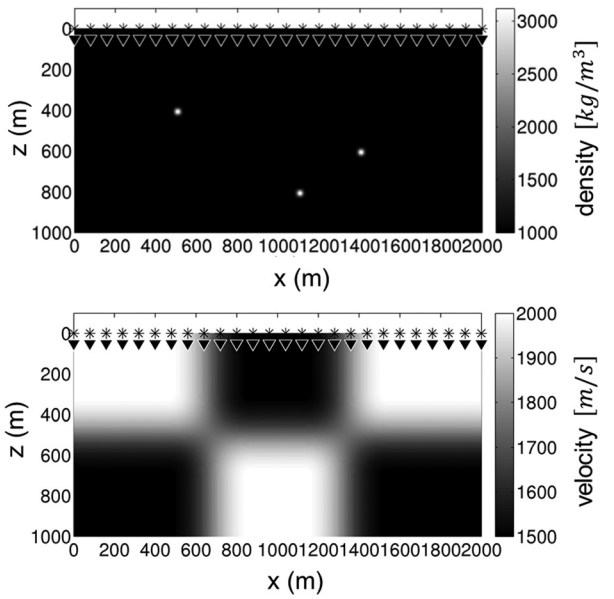

FIG. 9. Density (top) and velocity (bottom) distribution in a 3-diffractors model with a heterogeneous background structure. Symbol key as in Fig. 1. Only every fourth receiver and source is plotted for clarity. Scatterers are modeled as sharp density contrasts in a homogeneous background, whereas smooth checkerboard-like heterogeneities comprise the non-diffracting velocity distribution.

to-signal ratios (Fig. 8). One point of weakness in the algorithm is that a suitable detection threshold must be found that discriminates cross-correlations of primaries from those of multiply diffracted waves, based on the amplitude of the cross-correlation coefficient [e.g., Φ in Fig. 4(b)]. If diffractors are distributed widely across the medium, the amplitudes of primary diffractions can vary significantly (in the order of a factor of 10 in our study). The threshold needs to be set sufficiently low to enable detection of the weaker primaries. On the other hand, if diffractors are located close together, multiply diffracted waves can have relatively large amplitudes, and the threshold needs to be high enough so as not to mistake them for primaries. However, if the move-out of a multiply diffracted event is erroneously identified as a primary, it must in fact be identical to one of the primary move-outs but with a larger absolute arrival time. Comparing the move-outs thus allows one to reject those related to multiply diffracted waves that are simply later repetitions of other detected earlier-arriving move-outs. This can therefore be used as a criterion to set the detection threshold automatically: It should be chosen low enough that setting it to lower values yields no new and distinct move-outs, and large enough that no multiples are mistaken for primaries.

To our knowledge, the only other techniques that identify and isolate individual diffraction move-outs in a multiply scattering medium are methods based on time-reversal such as those proposed by Prada and Fink (1994) and Montaldo *et al*. (2004). These methods, however, require a transducer array (collocated sources and receivers) that records and re-injects the scattered wavefield. In our method, while to predict the full scattering path both a source and a receiver array is needed (which do not have to be collocated), primary move-outs can in principle be identified and isolated using only a receiver array that records the response from two separate sources. More sources can be used to improve the identified travel-time curves, but a densely sampled source array is not required.

The crucial step in the algorithm is the identification of secondaries. This step becomes more challenging the more diffractors are involved. The number of events that have been scattered m times in a medium containing n diffractors is $n*(n-1)^{m-1}$, hence, we expect n primaries (since $m=1$) and $n*(n-1)$ secondaries ($m=2$). This means that for $n=3$, as in the examples shown earlier, the number of secondaries is only 6, but for $n=5$ the number of secondaries is already 20.

As an aside, note that in an elastic medium, where both compressional (P) waves and shear (S) waves propagate, waves are converted every time they scatter. In theory, the assumption of a unique fingerprint for each diffractor still holds, the difference being that the elastic fingerprint consists of *two* travel-time curves in each data gather, one for the P-wave primary and one for the S-wave primary. Thus, assuming that the source generates only P-waves, the number of

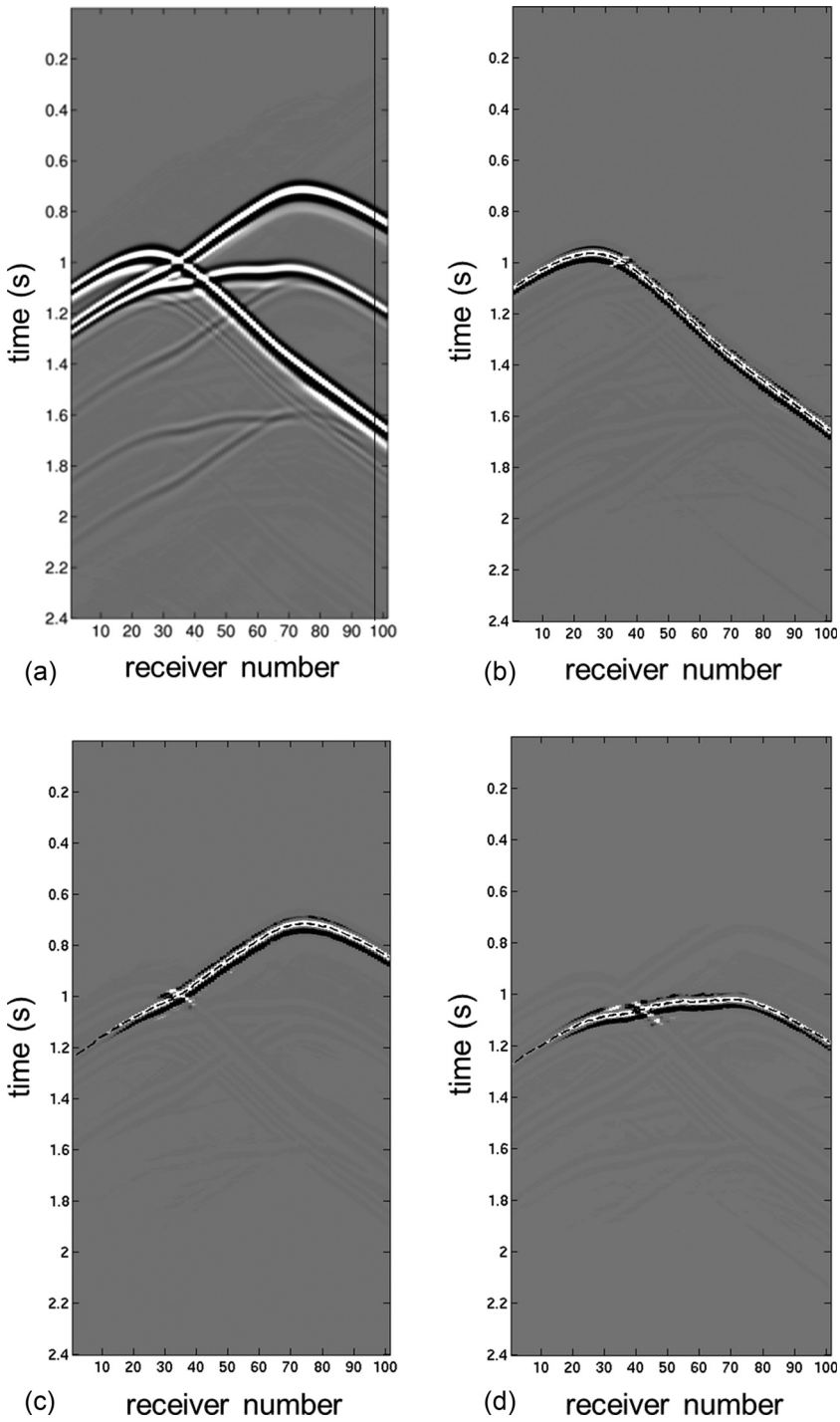

FIG. 10. (a) CSG obtained from the model in Fig. 9 with the common source located at [600 m, 0 m]. The vertical bold line marks the mutual trace. (b), (c) and (d): Cross-gathers showing primary move-outs estimated from the CSG in (a). Estimated travel-time curve are superimposed as dashed lines.

primaries doubles while the number of secondaries becomes four times as large compared to the acoustic case. We have not tested the elastic case but assume that performance would deteriorate.

Figure 8 shows that when the number of diffractors increases, the detected arrival times of secondaries are indeed increasingly error-prone. The sources of this error are discussed as follows. A prerequisite for the identification of secondary move-outs is the correct estimation of primary travel-time curves along which the semblance analysis is performed. If the extracted curve deviates from the true travel-time curve, computed semblance values are lower and may fall below the threshold for secondary detection. The results for primaries suggest that almost all primaries are identified correctly on the mutual trace. Note, however, that the estimated travel time was compared to the true travel time on the mutual trace only, which does not mean that the travel times are correct everywhere along the estimated curve. Errors in primary travel-time curves can be produced by an unfortunate combination of gathers, in which the travel-time shift of a move-out is not unique, i.e., two or more move-outs experience the same travel-time shift due to the spatial shift of the common source or the common receiver. This is more likely to happen, the more primaries

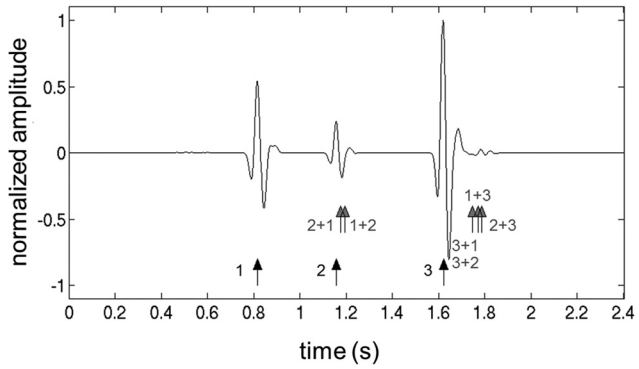

FIG. 11. Mutual trace of the CSG and CRG obtained from the 3-diffractors example with heterogeneous background velocity structure [Figs. 9 and 10(a)]. The maximum amplitude has been normalized to one. Arrows and numbers mark the arrivals of estimated primaries (black text) and secondaries (gray text). In this example the algorithm detected all primaries and secondaries correctly (Tables III and IV), i.e., the deviation from the true arrival time was below half the length of a wavelet (0.072 s).

there are in the data, and hence the more diffractors there are in the medium. This error thus has a larger impact for larger numbers of diffractors.

The accuracy with which travel times of tertiaries and higher-order scattered waves are predicted depends on the errors in the estimated primary and secondary travel times. Since these errors propagate through the algorithm, travel-time prediction gets less accurate with increasing scattering order: Let $F_{t(B)}$ be the absolute error (uncertainty) of the travel time of the primary from scatterer B, $F_{t(AB)}$ the absolute error of the travel time of secondary AB, and $F_{t(BC)}$ the absolute error of the travel time of secondary BC, then the absolute error of the predicted tertiary ABC is given by $F_{t(ABC)} = F_{t(AB)} + F_{t(B)} + F_{t(BC)}$. Similarly, the errors of tertiaries contribute to the errors of fourth order scattered events, and so on. In this study the prediction was limited to fourth order scattering where most events were still recognizable as individual, distinct arrivals. Just as in the algorithm of Meles and Curtis (2014a), this means that in principle the propagation of error could be corrected at each iteration if a clearly identifiable arrival on the trace can be associated with the predicted higher-order scattering event: The predicted arrival time may simply be replaced by the observed arrival time. This assumes that the initial errors in primaries and secondaries are sufficiently small that the correct higher-order event is identified.

As we move to higher and higher-order scattering, more events become superimposed or merged into a continuous coda, and the predicted travel times can no longer be related

TABLE III. Comparison of estimated (t_{est}) and true travel times (t_{true}) of primary arrivals on the mutual trace in the 3-diffractors example with a heterogeneous background velocity structure (Fig. 11). All estimated travel times lie within the permitted deviation of half the length of a wavelet (0.072 s).

Primary	t_{est}	t_{true}	$\lvert t_{\text{est}} - t_{\text{true}}\rvert$
1	0.82 s	0.82 s	0.00 s
2	1.16 s	1.16 s	0.00 s
3	1.63 s	1.62 s	0.01 s

TABLE IV. Comparison of estimated (t_{est}) and true travel times (t_{true}) of secondary arrivals on the mutual trace in the 3-diffractors example with a heterogeneous background velocity structure (Fig. 11). All estimated travel times lie within the permitted deviation of half the length of a wavelet (0.072 s).

Secondary	t_{est}	t_{true}	$\lvert t_{\text{est}} - t_{\text{true}}\rvert$
2 + 1	1.18 s	1.22 s	0.03 s
1 + 2	1.20 s	1.24 s	0.04 s
3 + 1	1.75 s	1.74 s	0.02 s
3 + 2	1.75 s	1.79 s	0.04 s
1 + 3	1.78 s	1.82 s	0.04 s
2 + 3	1.79 s	1.85 s	0.05 s

to individual arrivals. Also, for most applications (e.g., diffraction imaging) considering low-order scattering will be sufficient, especially as our method demonstrates explicitly that theoretically all kinematic information is contained in primaries and secondaries.

In models with three or more diffractors the superposition of primaries and secondaries on the mutual trace can lead to ambiguity and hence misinterpretation. When, for example, primary A coincides with secondary $B + C$, two different move-outs intersect in each gather: Move-outs A and B in the CRG (fingerprints of the first diffractors), and move-outs A and C in the CSG (fingerprints of the last diffractors). After the algorithm has detected all move-outs, it then identifies *four* possible combinations of first and last fingerprints: $A + A$, which corresponds to primary A; $B + C$, which corresponds to the true secondary; and two false events, namely the secondaries $A + C$ and $B + A$. This ambiguity is more likely to occur the more diffractors there are in the model, and hence the more fingerprints overlap in the data gathers. Note that the superposition of primary arrivals, which is another potential source of misinterpretation, is avoided automatically by the algorithm through the appropriate selection of the gathers to be analyzed.

As we would expect, Fig. 8 also shows that the secondary detection in general deteriorates when the noise-to-signal ratio is increased. A considerable drop is observed for noise-to-signal ratios of 3 and higher, which means that the average noise amplitude is at least 3 times as large as the typical amplitude of a secondary arrival. We interpret this as the point where the coherency of the multiply scattered arrivals is completely extinguished by the incoherent noise field. Before this point, larger noise levels may affect the accuracy of the extracted primary travel-time curves, which results in minor errors in the semblance analysis. Also, the threshold used to distinguish multiply scattered waves from background noise (defined as the mean of the semblance vector) may not be suitable for all noise-to-signal ratios.

Figure 8 implies that in some cases the algorithm returns better results when the noise level is higher. This unexpected pattern of performance (improvement with noisier data) can be explained by a problem that mainly affects low noise data, where move-outs of higher-order multiples may also be observed in the data with similar amplitudes to secondaries. Superposition of these arrivals with primary or secondary arrivals on the mutual trace causes similar ambiguities as

described above. For noisier data these higher-order multiples are not detected due to their relatively small amplitudes compared to the noise levels and this source of error is avoided, which results in more accurate detection of secondaries.

Inherent ambiguities due to the simultaneous arrival of different events cannot be solved on the basis of a single trace. However, we have the option to consult new (perhaps neighboring) mutual traces in the data cube, analyze the corresponding CRG and CSG, and compare the results. In this case source-receiver interferometry operations can be used to re-datum the estimated arrival times to the old source and receiver positions (Curtis and Halliday, 2010; Halliday and Curtis, 2010; Curtis *et al*., 2012) and thus to compare arrivals on two different traces directly. If the results are inconsistent, more traces must be analyzed in order to decide between them on a statistical basis. Experimental results suggest that the choice of the trace has a considerable impact on results, which can in fact be more significant than the effect of the noise level.

The problems described above occur especially for larger numbers of diffractors since with increasing complexity of the wavefield the identification of secondaries becomes more difficult. Nevertheless, for a small number of strong diffractors we have demonstrated that a development of the method by Meles and Curtis (2014a) can be automated, and have successfully applied it to synthetic acoustic noisy data. Future research should test its applicability to real data sets, for example, from an acoustic laboratory experiment or field data. The method could eventually find application in improved diffractor localization by using multiples, or to provide new information about inter-diffractor paths. One important transferable learning that both Meles and Curtis (2014a) and this work demonstrate is that in theory all travel time information in the multiply-diffracted wavefield is in fact included in only the primary and secondary arrivals. This implies, for example, that since the travel times of higher order scattered waves are explicitly related to order one and two waves, observations of higher order travel times might be used to improve estimates of lower order travel times.

Moreover, the identification and isolation of primary events by computing cross-gathers and evaluating the energy distribution in these gathers could be a useful method in its own right. Since it is entirely non-parametric (and can therefore identify entirely non-hyperbolic move-outs) it can also be applied to more generally heterogeneous velocity structures, as demonstrated in Fig. 10. This may be of interest for a variety of data processing operations, for example in travel-time tomography or event-based filtering.

Finally, while all of our tests have been in 2D models, there is an obvious extension of the method to three-dimensional (3D) models using planes rather than lines of receivers by simply allowing parameter n in the above equations to index over the plane rather than only a line. In fact, this may improve rather than diminish performance for any particular number of diffractors, because there would usually then be far more data to discriminate between different move-outs, and because planes of receivers allow move-outs to be discriminated in two spatial directions rather than only in one. Thus the method might be usefully applied in applications where one can only access one side of a 3D medium.

ACKNOWLEDGMENTS

We thank the Edinburgh Interferometry Project sponsors (ConocoPhillips, Schlumberger Cambridge Research, Statoil, and Total) for supporting this research and granting us permission to publish it. We thank Roel Snieder and Deyan Draganov for their constructive comments, which helped improve the manuscript.

Aubry, A., and Derode, A. (**2010**). "Multiple scattering of ultrasound in weakly inhomogeneous media: Application to human soft tissue," J. Acoust. Soc. Am. **129**, 225–233.

Bordier, J. M., Fink, M., Le Brun, A., and Cohen-Tenoudji, F. (**1991**). "The influence of multiple scattering in incoherent ultrasonic inspection of course grain stainless steel," *Ultrasonics Symposium*, pp. 803–808.

Born, M., and Wolf, E. (**1999**). *Principles of Optics*, 7th ed. (Cambridge University Press, Cambridge, UK), Chap. 8, pp. 412–425.

Brekhovskikh, L. M., and Lysanov, Y. P. (**2003**). *Fundamentals of Ocean Acoustics* (Springer-Verlag, New York), Chap. 11, pp. 250–264.

Curtis, A., Behr, Y., Entwistle, E., Galetti, E., Townend, J., and Bannister, S. (**2012**). "The benefit of hindsight in observational science: Retrospective seismological observations," Earth Planet. Sci. Lett. **345**, 212–220.

Curtis, A., and Halliday, D. (**2010**). "Source-receiver wavefield interferometry," Phys. Rev. E **81**, 046601.

De Rosny, J., and Roux, P. (**2001**). "Multiple scattering in a reflecting cavity: Application to fish counting in a tank," J. Acoust. Soc. Am. **109**, 2587–2597.

Ferretti, A., Prati, C., and Rocca, F. (**2001**). "Permanent scatterers in SAR interferometry," IEEE Trans. Geosci. Remote Sensing **39**, 8–20.

Fink, M., Montaldo, G., and Tanter, M. (**2003**). "Time-reversal acoustics in biomedical engineering," Annu. Rev. Biomed. Eng. **5**, 465–497.

Foldy, L. L. (**1945**). "The multiple scattering of waves. I. General theory of isotropic scattering by randomly distributed scatterers," Phys. Rev. **67**, 107–119.

Foote, K. G. (**2008**). "Acoustic scattering by marine organisms," in *Encyclopedia of Ocean Sciences*, 2nd ed. (Academic Press, London), pp. 62–70.

Friedrich, H. (**2006**). *Theoretical Atomic Physics* (Springer-Verlag, New York), Vol. 3, Chap. 2.

Galetti, E., Halliday, D., and Curtis, A. (**2013**). "A simple and exact acoustic wavefield modeling code for data processing, imaging and interferometry applications," Geophysics **78**, F17–F27.

Gao, L. S., Lee, L. C., Biswas, N., and Aki, K. (**1983**). "Comparison of the effects between single and multiple scattering on coda waves for local earthquakes," Bull. Seismol. Soc. Am. **73**, 1943–3573.

Halliday, D. F., and Curtis, A. (**2009**). "Generalized optical theorem for surface waves and layered media," Phys. Rev. E **79**, 056603.

Halliday, D., and Curtis, A. (**2010**). "An interferometric theory of source-receiver scattering and imaging," Geophys. **75**(6), SA95–SA103.

Halliday, D. F., Curtis, A., Vermeer, P., Strobbia, C., Glushchenko, A., van Manen, D. J., and Robertsson, J. O. (**2010**). "Interferometric ground-roll removal: Attenuation of scattered surface waves in single-sensor data," Geophysics **75**(2), SA15–SA25.

Harmankaya, U., Kaslilar, A., Thorbecke, J., Wapenaar, K., and Draganov, D. (**2013**). "Locating near-surface scatterers using non-physical scattered waves resulting from seismic interferometry," J. Appl. Geophys. **91**, 66–81.

Insana, M. F., Wagner, R. F., Brown, D. G., and Hall, T. J. (**1990**). "Describing small-scale structure in random media using pulse-echo ultrasound," J. Acoust. Soc. Am. **87**, 179–192.

Jixiang, X., McLean, B. F., and Xuejuan, S. (**2014**). "A near-surface seismic scattered wave separation method," Adv. Pet. Explor. Dev. **41**(6), 771–777.

Kaslilar, A., Harmankaya, U., van Wijk, K., Wapenaar, K., and Draganov, D. (**2014**). "Estimating location of scatterers using seismic interferometry of scattered Rayleigh waves," Near Surface Geophys. **12**(6), 721–730.

Khaidukov, V., Landa, E., and Moser, T. J. (**2004**). "Diffraction imaging by focusing-defocusing: An outlook on seismic super resolution," Geophys. **69**, 1478–1490.

Landa, E., Shtivelman, V., and Gelchinsky, B. (**1987**). "A method for detection of diffracted waves on common-offset sections," Geophys. Prospect. **35**, 359–374.

Larose, E., de Rosny, J., Margerin, L., Anache, D., Gouedard, P., Campillo, M., and van Tiggelen, B. (**2006**). "Observation of multiple scattering of kHz vibrations in a concrete structure and application to monitoring weak changes," Phys. Rev. E **73**, 016609.

Meles, G. A., and Curtis, A. (**2014a**). "Fingerprinting ordered diffractions in multiply-scattered waves," Geophys. J. Int. **198**, 1701–1713.

Meles, G. A., and Curtis, A. (**2014b**). "Discriminating physical and non-physical diffracted energy in source-receiver interferometry," Geophys. J. Int. **197**, 1642–1659.

Montaldo, G., Tanter, M., and Fink, M. (**2004**). "Revisiting iterative time reversal processing: Application to detection of multiple targets," J. Acoust. Soc. Am. **115**, 776–784.

Pacheco, C., and Snieder, R. (**2006**). "Time-lapse traveltime change of singly scattered acoustic waves," Geophys. J. Intl. **165**(2), 485–500.

Papziner, U., and Nick, K. P. (**1998**). "Automatic detection of hyperbolas in georadargrams by slant-stack processing and migration," First Break **16**, 219–223.

Prada, C., and Fink, M. (**1994**). "Eigenmodes of the time-reversal operator: A solution to selective focusing in multiple-target media," Wave Motion **20**, 151–163.

Prada, C., Kerbrat, E., Cassereau, D., and Fink, M. (**2002**). "Time reversal techniques in ultrasonic nondestructive testing of scattering media," Inverse Probl. **18**, 1761–1773.

Sheriff, R. E., and Geldart, L. P. (**1995**). *Exploration Seismology*, 2nd ed. (Cambridge University Press, Cambridge, UK), Chap. 9, pp. 288–289.

Stanton, T. K. (**1982**). "Multiple scattering with applications to fish-echo processing," J. Acoust. Soc. Am. **73**, 1164–1169.

Tadayyon, H., Sadeghi-Naini, A., Wirtzfeld, L., Wright, F. C., and Czarnota, G. (**2014**). "Quantitative ultrasound characterization of locally advanced breast cancer by estimation of its scatterer properties," Med. Phys. **41**, 012903.

Thorson, R., and Claerbout, J. F. (**1985**). "Velocity-stack and slant-stack stochastic inversion," Geophys. **50**, 2727–2741.

Wu, R., and Aki, K. (**1988**). "Introduction: Seismic wave scattering in three-dimensionally heterogeneous earth," in *Scattering and Attenuations of Seismic Waves, Part I* (Birkhäuser Verlag, Basel), pp. 1–6.